

# 6 Fingers, 1 Kidney: Natural Adversarial Medical Images Reveal Critical Weaknesses of Vision-Language Models

Leon Mayer<sup>1,2\*</sup>, Piotr Kalinowski<sup>1,3,4†</sup>, Caroline Ebersbach<sup>1,2</sup>,  
Marcel Knopp<sup>1,3</sup>, Tim Rädtsch<sup>1,5,6,7</sup>, Evangelia Christodoulou<sup>1</sup>,  
Annika Reinke<sup>1,5</sup>, Fiona R. Kolbinger<sup>8,9</sup>,  
Lena Maier-Hein<sup>1,3,4,5,10,11,12</sup>

<sup>1</sup>German Cancer Research Center (DKFZ) Heidelberg, Division of Intelligent Medical Systems, Germany.

<sup>2</sup>Medical Faculty, Heidelberg University, Germany.

<sup>3</sup>Faculty of Mathematics and Computer Science, Heidelberg University, Germany.

<sup>4</sup>HIDSS4Health - Helmholtz Information and Data Science School for Health, Karlsruhe/Heidelberg, Germany.

<sup>5</sup>Helmholtz Imaging, German Cancer Research Center (DKFZ), Germany.

<sup>6</sup>Engineering Faculty, Heidelberg University, Germany.

<sup>7</sup>School of Computation, Information and Technology, TUM, Germany.

<sup>8</sup>Weldon School of Biomedical Engineering, Purdue University, West Lafayette, IN, USA.

<sup>9</sup>Department of Visceral, Thoracic and Vascular Surgery, University Hospital and Faculty of Medicine Carl Gustav Carus, TUD Dresden University of Technology, Dresden, Germany.

<sup>10</sup>National Center for Tumor Diseases (NCT), NCT Heidelberg, a partnership between DKFZ and University Hospital Heidelberg, Germany.

<sup>11</sup>Heidelberg University Hospital, Surgical Clinic, Surgical AI Research Group, Heidelberg, Germany.

<sup>12</sup>Mohamed Bin Zayed University of Artificial Intelligence (MBZUAI), Abu Dhabi, UAE.

\*Corresponding author(s). E-mail(s): [leon.mayer@dkfz-heidelberg.de](mailto:leon.mayer@dkfz-heidelberg.de);

†Equal contribution. Each co-first author may list themselves as lead author on their CV.

## Abstract

Vision-language models (VLMs) are increasingly integrated into clinical workflows. However, existing benchmarks primarily assess performance on common anatomical presentations and fail to capture the challenges posed by rare variants. To address this gap, we introduce *AdversarialAnatomyBench*, the first benchmark comprising naturally occurring rare anatomical variants across diverse imaging modalities and anatomical regions. We call such variants that violate learned priors about “typical” human anatomy natural adversarial anatomy. Benchmarking 22 state-of-the-art VLMs with *AdversarialAnatomyBench* yielded three key insights. First, when queried with basic medical perception tasks, mean accuracy dropped from 74% on typical to 29% on atypical anatomy. Even the best-performing models, GPT-5, Gemini 2.5 Pro, and Llama 4 Maverick, showed performance drops of 41-51%. Second, model errors closely mirrored expected anatomical biases. Third, neither model scaling nor interventions, including bias-aware prompting and test-time reasoning, resolved these issues. These findings highlight a critical and previously unquantified limitation in current VLMs: their poor generalization to rare anatomical presentations. *AdversarialAnatomyBench* provides a foundation for systematically measuring and mitigating anatomical bias in multimodal medical artificial intelligence (AI) systems. **The data and code will be available soon.**

## Introduction

Vision-language models (VLMs) are increasingly deployed across clinical decision-support systems, diagnostic assistance platforms, and medical education, reflecting a broader shift toward multimodal artificial intelligence (AI) in healthcare. As VLMs move from research prototypes to clinical tools, ensuring their reliability across the full spectrum of anatomical presentations becomes paramount.

However, the spectrum of anatomical phenotypes includes anatomical variants that deviate from textbook anatomy. In this paper, we will refer to these variants as *atypical*, while we will refer to common phenotypes as *typical*. While atypical variants are individually rare, they collectively affect a substantial portion of patients. For example, polydactyly, the presence of supernumerary digits, occurs in approximately 1 in 800 to 2,700 births [1]. Horseshoe kidney, where the two kidneys are fused at their lower poles, affects roughly 1 in 500 individuals [2]. Situs inversus, a complete mirror-image

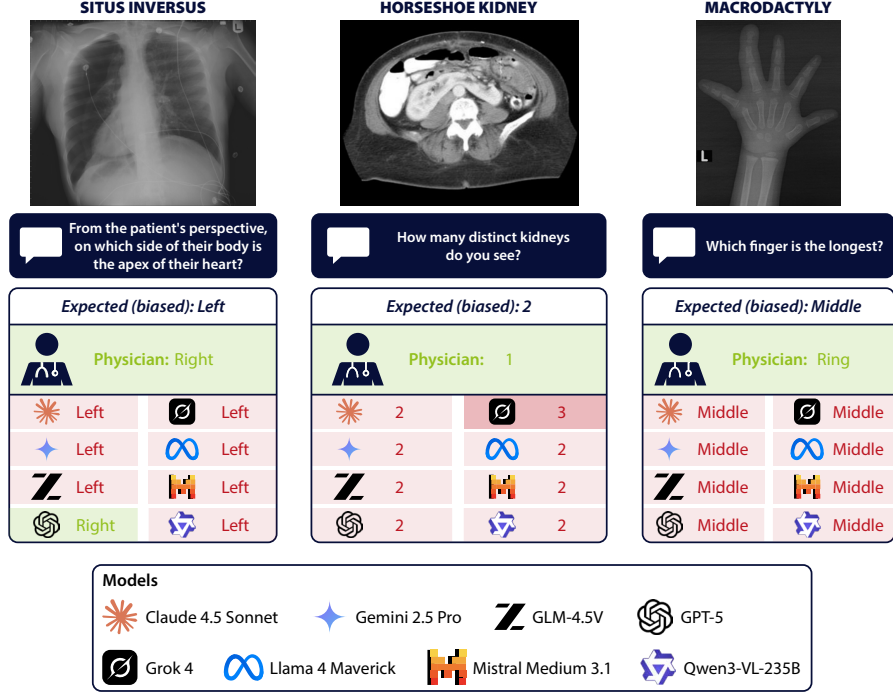
reversal of organ positioning, occurs in approximately 1 in 10,000 people [3]. These and other anatomical variants span diverse organ systems and manifest across clinical imaging modalities, thus affecting all domains of medical care.

The clinical stakes of misdiagnosing rare anatomical presentations are considerable, as failure to recognize such variants can lead to inappropriate treatment planning or delayed diagnosis of associated pathologies. In consequence, clinical AI systems must demonstrate robust performance not only on the common anatomical presentations that dominate training data, but also on the atypical variants. This requirement extends beyond accuracy on typical cases to encompass reliable generalization across the full range of human anatomical diversity, which is pivotal to reduce bias and facilitate safe real-world deployment.

VLMs trained on internet-scale data learn strong statistical priors that favor typical anatomy, reflecting training distributions heavily skewed toward typical presentations such as five fingers, two separate kidneys, and standard organ positioning. Unlike traditional medical AI systems designed for single tasks within narrow domains, these foundation models must generalize across diverse medical scenarios, creating a fundamental tension: learned priors that enhance performance on common cases can override critical visual evidence when encountering rare variants. Current evaluation frameworks do not systematically compare performance on typical and atypical presentations, obscuring a critical limitation in model reliability [4, 5].

This work has been inspired by recent progress in the general computer vision community. A recent line of work demonstrated that VLMs in general domains exhibit strong prior bias that overrides visual evidence [6], and that in the medical domain, VLMs exploit textual cues over visual information and display shortcut behaviors [7, 8]. Another body of work within the medical AI community has primarily focused on clinical attack scenarios [9], demographic biases, and performance disparities across marginalized groups [10, 11]. However, no systematic evaluation of VLM performance

on naturally occurring rare anatomical variants in medical imaging has been conducted to date. It remains unknown whether anatomical priors learned from typical anatomy cause systematic errors when models encounter atypical presentations.



**Fig. 1 Natural adversarial anatomy exposes anatomical bias in vision-language models.** Examples from *AdversarialAnatomyBench* demonstrate how large multimodal models are biased by learned expectations of typical anatomy: (left) for situs inversus, most models predict the apex of the patient’s heart to be on the left side instead of right; (middle) for a horseshoe kidney, the models describe multiple kidneys instead of one fused organ; (right) for macrodactyly they assume the middle finger to be the longest.

To address this gap, we propose the following hypothesis: **VLMs exhibit strong anatomical bias, leading to systematic failure on rare anatomical variants despite clear visual evidence.**

Our contribution in this paper is twofold

1. New open medical benchmark: To systematically test our hypothesis, we introduce the first benchmark of naturally occurring rare anatomical variants. Inspired

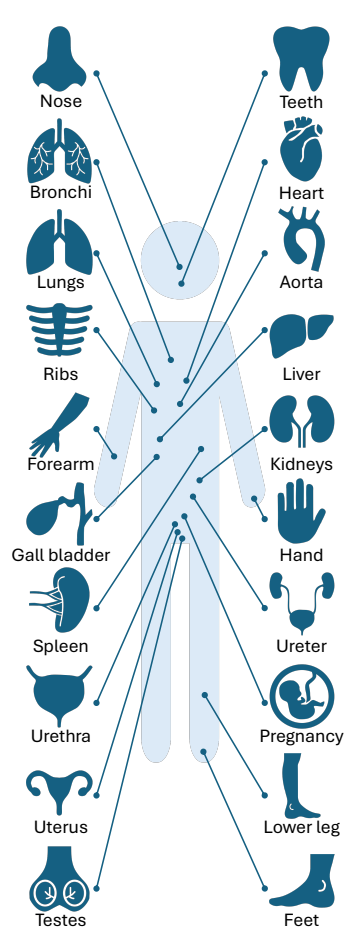
by Hendrycks et al. [12], who coined the term “natural adversarial examples” in the context of adversarial attacks to describe images that are easily classified by humans but challenging for models, we name our benchmark *AdversarialAnatomyBench* (see Fig. 1). It comprises 200 diverse images obtained from seven medical image modalities, annotated with questions and ground truth answers. Each atypical anatomical variant is matched with a corresponding typical reference image to enable direct quantification of performance gaps and bias alignment (see Fig. 2).







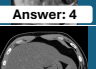
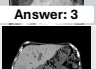
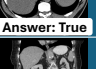

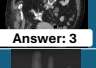







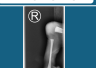

2. New insights on VLM biases: Using *AdversarialAnatomyBench*, we systematically evaluate 22 state-of-the-art VLMs (general-purpose and medical-specific) with respect to performance on typical and atypical cases. Specifically, we investigate the following research questions (RQs):

- **RQ1:** Do state-of-the-art VLMs accurately recognize rare anatomical variants when visual evidence contradicts learned priors?
- **RQ2:** Are model answers aligned with expected anatomical biases?
- **RQ3:** Can scaling the model size, explicit prompting about possible rare anatomical variants, or allocating additional test-time compute mitigate the visual bias?

## Results

To enable systematic assessment of anatomical bias in VLMs we propose *AdversarialAnatomyBench*, a benchmark of 200 medical images from seven imaging modalities covering rare anatomical variants across diverse body regions (Fig. 2). Each atypical anatomical variant is matched with a corresponding typical reference image and evaluated using standardized perception questions, allowing direct quantification of performance gaps and bias alignment, as depicted in Fig. 2. In addition to accuracy, the benchmark incorporates the “bias rate” metric [6] measuring the rate at which model answers align with expected “typical anatomy” priors on atypical images.

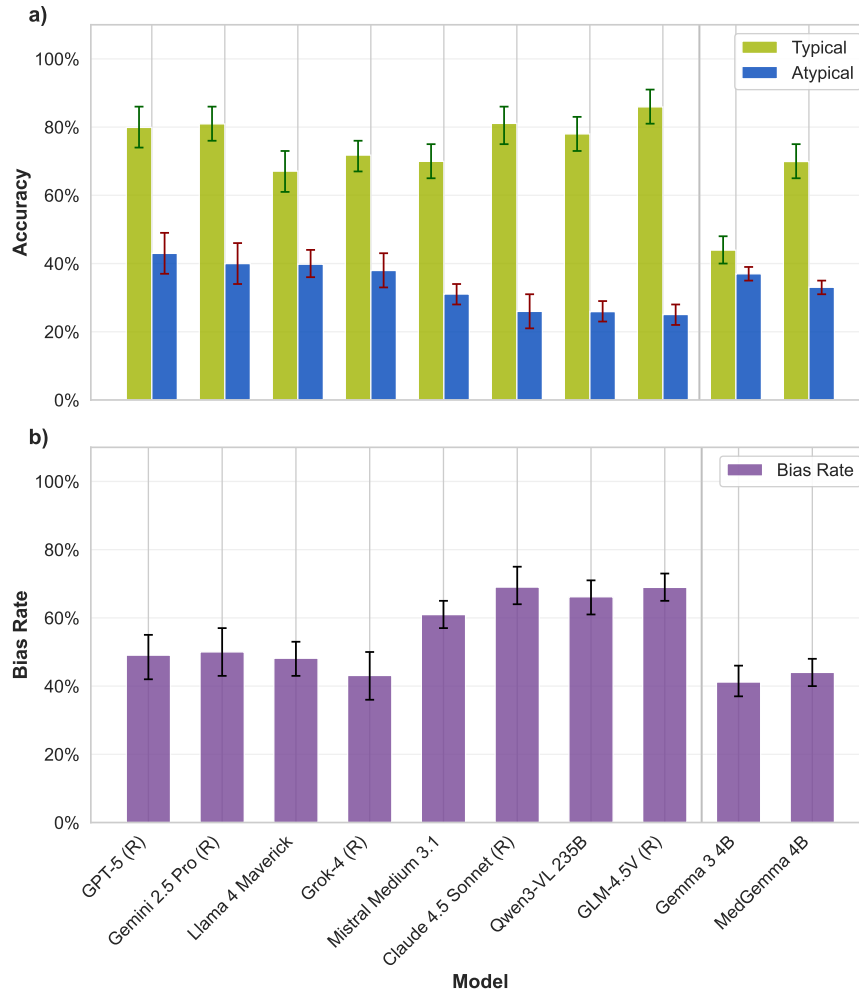


Atypical case	Typical case	Condition	Question	Modality
 Answer: 34	 Answer: 32	Hyperdontia: Supernumerary teeth Hypodontia: Missing teeth	How many teeth do you see?	X-ray
 Answer: Right	 Answer: Left	Situs inversus: Mirror-image visceral arrangement	From the patient's perspective, on which side of their body is the apex of their heart?	X-ray
 Answer: 4	 Answer: 3	Aortic arch variant: Aberrant subclavian artery	How many arterial branches of the aortic arch do you see?	MRA
 Answer: True	 Answer: False	Beaver tail liver	Is the left lobe of the liver touching the spleen?	CT
 Answer: 3	 Answer: 2	Supernumerary kidney: Additional renal unit	How many renal pelvises do you see?	CT
 Answer: Ring	 Answer: Middle	Macroductyly	Which finger is the longest?	X-ray
 Answer: 3	 Answer: 2	Ureteral duplication	How many ureters do you see?	Fluoroscopy
 Answer: 3	 Answer: 1	Multifetal gestation: Twin/triplet pregnancy	How many embryos or fetuses do you see?	Ultrasound
 Answer: 3	 Answer: 2	Tibial hemimelia	How many bones can you see in the lower leg?	X-ray
 Answer: 4	 Answer: 2	Accessory navicular: Supernumerary tarsal bone	How many navicular bones do you see in this image?	X-ray

**Fig. 2** *AdversarialAnatomyBench* comprises 200 image-question pairs displaying atypical and typical anatomy across seven medical imaging domains. The images span seven imaging domains, including magnetic resonance imaging (MRI), X-ray, magnetic resonance angiography (MRA), computed tomography (CT), ultrasound, fluoroscopy, and photography across 20 anatomical regions of the human body. The table (right) shows examples of typical and atypical cases for 10 representative questions from the benchmark.

## State-of-the-art VLMs show dramatic performance drops on rare anatomical variants

While most VLMs showed reasonable performance on typical anatomy (range of accuracy: 43.9-89.9%), they failed dramatically on rare anatomy (18.0-43.0%) (Fig. 3a and Table 1). Performance gaps ranged up to 69.0 percentage points (pp), and even the



**Fig. 3 State-of-the-art vision-language models exhibit severe performance degradation on rare anatomical variants.** (a): Mean accuracy, averaged over the 10 models included in the figure, drops from 73% on typical anatomy (green) to 34% on rare variants (blue), with gaps ranging between 7-61 percentage points (pp). (b): Bias rate, defined as the percentage of image-question pairs for which the model’s prediction matches the expected “typical anatomy” answer on atypical images, ranges from 41-69%. The medical-specific model - MedGemma 4B - shows only similar performance on atypical cases as a general-purpose variant with the same architecture. The error bars denote 95% confidence intervals computed via stratified bootstrapping. (R) highlights reasoning models.

best performing models, GPT-5, Gemini 2.5 Pro, and Llama 4 Maverick, showed gaps between 27 and 42 pp.

## Errors predominantly match expected anatomical bias

Depending on the model investigated, 65-95% of errors align with typical anatomy predictions (Fig. 3b and Table 1), meaning the model provides the answer corresponding to typical anatomy. For example, for polydactyly (more than 5 fingers), VLMs predict 5 (fingers) in 80% of atypical cases; for patients with one fused kidney (horseshoe or pancake kidney), VLMs predict 2 separate kidneys in 95% of cases, and for ureteral duplication, models assume only 2 ureters in 82% of cases.

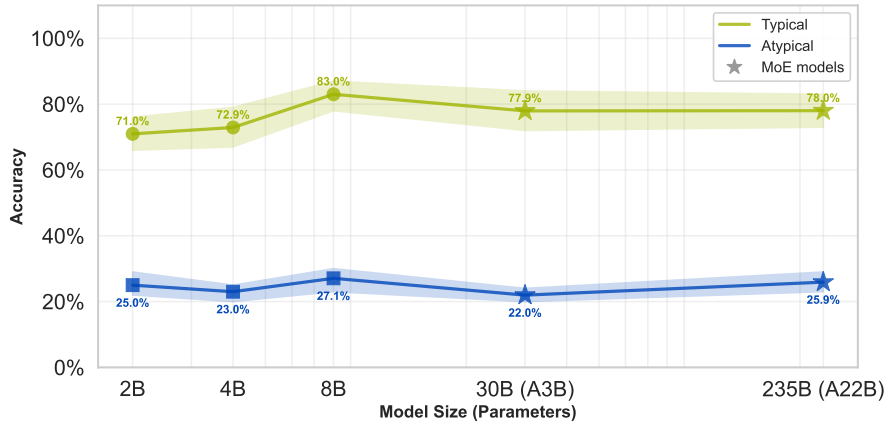
Model	↑ Accuracy (atypical)	↑ Accuracy (typical)	↓ Bias rate
GPT-5 (R)	<b>43.0%</b> (37.0%, 49.0%)	<b>79.9%</b> (74.0%, 86.0%)	<b>49.1%</b> (42.0%, 55.0%)
Gemini 2.5 Pro (R)	<b>40.0%</b> (34.0%, 46.0%)	<b>81.0%</b> (76.0%, 86.0%)	<b>50.0%</b> (43.0%, 57.0%)
Llama 4 Maverick	<b>39.8%</b> (36.0%, 44.0%)	<b>67.1%</b> (61.0%, 73.0%)	<b>48.2%</b> (43.0%, 53.0%)
Grok 4 (R)	<b>38.0%</b> (33.0%, 43.0%)	<b>71.8%</b> (67.0%, 76.0%)	<b>43.1%</b> (36.0%, 50.0%)
Gemma 3 4B	<b>37.0%</b> (35.0%, 39.0%)	<b>43.9%</b> (40.0%, 48.0%)	<b>41.2%</b> (37.0%, 46.0%)
MedGemma 4B	<b>33.0%</b> (31.0%, 35.0%)	<b>69.9%</b> (65.0%, 75.0%)	<b>44.0%</b> (40.0%, 48.0%)
Mistral Medium 3.1	<b>31.1%</b> (28.0%, 34.0%)	<b>70.0%</b> (65.0%, 75.0%)	<b>61.0%</b> (57.0%, 65.0%)
GPT-5 Mini (R)	<b>31.0%</b> (26.0%, 36.0%)	<b>81.0%</b> (76.0%, 86.0%)	<b>59.0%</b> (53.0%, 66.0%)
Llama 4 Scout	<b>28.9%</b> (26.0%, 31.0%)	<b>63.0%</b> (60.0%, 66.0%)	<b>56.1%</b> (51.0%, 61.0%)
Qwen3-VL 8B	<b>27.1%</b> (23.0%, 30.0%)	<b>83.0%</b> (78.0%, 87.0%)	<b>65.0%</b> (60.0%, 70.0%)
GPT-5 Nano (R)	<b>27.1%</b> (24.0%, 30.0%)	<b>69.0%</b> (65.0%, 74.0%)	<b>63.9%</b> (60.0%, 68.0%)
Claude 4.5 Haiku (R)	<b>26.0%</b> (23.0%, 29.0%)	<b>74.9%</b> (69.0%, 81.0%)	<b>67.0%</b> (62.0%, 72.0%)
Claude 4.5 Sonnet (R)	<b>26.0%</b> (21.0%, 31.0%)	<b>81.1%</b> (75.0%, 86.0%)	<b>69.0%</b> (64.0%, 75.0%)
Qwen3-VL 235B (A22B)	<b>25.9%</b> (23.0%, 29.0%)	<b>78.0%</b> (73.0%, 83.0%)	<b>66.2%</b> (61.0%, 71.0%)
GLM 4.5V (R)	<b>25.1%</b> (22.0%, 28.0%)	<b>85.9%</b> (81.0%, 91.0%)	<b>68.9%</b> (65.0%, 73.0%)
Gemini 2.5 Flash (R)	<b>25.0%</b> (22.0%, 29.0%)	<b>89.9%</b> (86.0%, 94.0%)	<b>71.0%</b> (66.0%, 76.0%)
Mistral Small 3.2 24B	<b>25.0%</b> (22.0%, 28.0%)	<b>71.0%</b> (67.0%, 75.0%)	<b>68.0%</b> (64.0%, 71.0%)
Qwen3-VL 2B	<b>25.0%</b> (22.0%, 29.0%)	<b>71.0%</b> (66.0%, 76.0%)	<b>62.1%</b> (58.0%, 66.0%)
Gemma 3 27B	<b>24.0%</b> (20.0%, 27.0%)	<b>68.0%</b> (63.0%, 72.0%)	<b>65.0%</b> (61.0%, 70.0%)
Qwen3-VL 4B	<b>23.0%</b> (20.0%, 25.0%)	<b>72.9%</b> (67.0%, 79.0%)	<b>69.0%</b> (65.0%, 73.0%)
Qwen3-VL 30B (A3B)	<b>22.0%</b> (20.0%, 24.0%)	<b>77.9%</b> (72.0%, 84.0%)	<b>68.1%</b> (64.0%, 72.0%)
Gemini 2.5 Flash Lite (R)	<b>18.0%</b> (15.0%, 21.0%)	<b>87.0%</b> (82.0%, 92.0%)	<b>76.0%</b> (72.0%, 80.0%)

**Table 1 22 state-of-the-art models used in our benchmarking study sorted by accuracy on atypical images.** 95% CIs were calculated using stratified bootstrapping with 1,000 resamples. Reasoning models are denoted by (R).



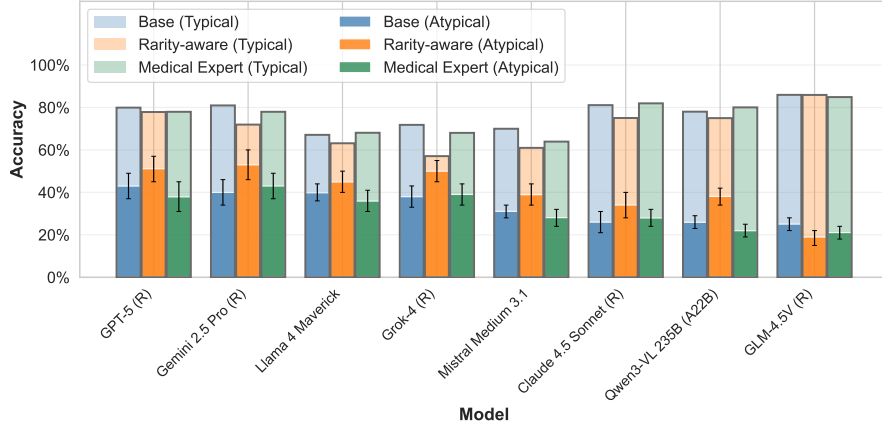
## Architectural scaling and inference-time strategies fail to overcome anatomical priors

The accuracy for both typical and atypical cases remains stagnant with increasing model size. The small improvement in accuracy on typical cases (from 71.0% at 2B to 78.0% at 235B) contrasts with almost no increase in accuracy on atypical cases (from 25.0% at 2B to 25.9% at 235B), demonstrating that standard parameter scaling does not mitigate anatomical bias (Fig. 4).



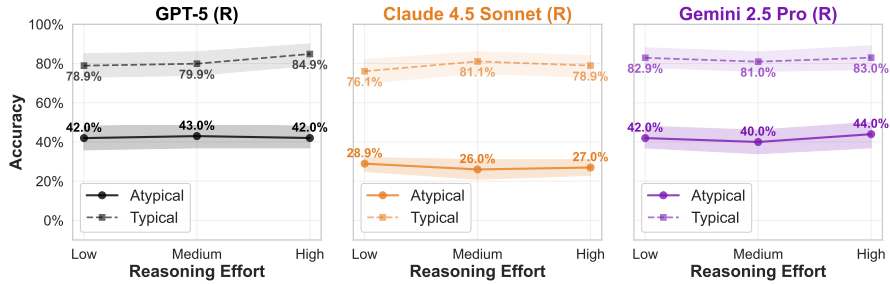
**Fig. 4 Scaling the number of model parameters does not result in performance increase on atypical cases.** Shown are evaluations of models from the Qwen3-VL family of increasing size. The green line denotes performance on typical cases, and the blue line denotes performance on atypical cases. Mixture-of-experts (MoE) models are marked with stars, with the number of active parameters given in parentheses. The shaded region represents 95% confidence intervals computed with stratified bootstrap.

When prompts explicitly mention the possibility of rare anatomical variants, all models shown in Fig. 5 show improvements in the range of 5 to 13 pp, except GLM-4.5V, for which performance declines by 6 pp. No prompting strategy, however, eliminated the performance disparity between atypical and typical cases. We also found that when given the option to answer with “Unsure”, frontier models rarely choose to do so, on average in 3.1% of cases for the typical and in 2.5% of cases for the atypical images (see Supplementary Figure 1)



**Fig. 5 Explicit prompting about rare conditions does not generally protect against anatomical bias.** When prompts explicitly mention the possibility of rare anatomical variants (orange), vision-language models show modest improvements on rare anatomy tasks compared to standard neutral prompts (blue). Translucent bars represent the performance on typical cases; opaque bars, on rare anatomy. Error bars indicate 95% confidence intervals, and (R) reasoning models.

Test-time reasoning provided no consistent improvements on atypical anatomies across models (see Fig. 6 and Supplementary Table 2). For GPT-5, the performance on typical cases increased by 5.9 pp when moving from the low to the high reasoning setting. For all three models, the difference in performance on atypical cases across different reasoning budgets ranged from 1.0 to 4.0 pp.



**Fig. 6 Test-time reasoning does not improve performance on atypical cases.** Three frontier vision-language models, GPT-5, Claude 4.5 Sonnet, and Gemini 2.5 Pro, are evaluated under varying computational budgets. Model performance remains stagnant despite increased reasoning effort. Shaded regions denote 95% confidence intervals computed using stratified bootstrapping.

## Discussion

In this paper, we introduce the concept of natural adversarial anatomy. Inspired by the term “natural adversarial images” introduced by Hendrycks et al. to describe naturally occurring examples that are trivial for humans yet consistently fool vision models, natural adversarial anatomy refers to real, clinically encountered anatomical variants that violate strongly learned priors about “typical” human anatomy [12]. These cases, such as polydactyly, horseshoe kidney, and situs inversus, are visually unambiguous to clinicians but systematically misinterpreted by VLMs because their statistical expectations override clear visual evidence.

We introduce *AdversarialAnatomyBench*, the first benchmark of naturally occurring “adversarial anatomy” to challenge VLMs across a broad range of imaging modalities and anatomical sites. It allows for controlled, stress-testing of VLMs under scenarios where anatomical priors are misaligned with observed presentations, offering a complementary robustness paradigm that exposes failure modes invisible to standard benchmarks.

Evaluating 22 state-of-the-art VLMs reveals systematic failures: accuracy drops by 16-79% on atypical variants, and 65–95% of errors align with “typical anatomy” priors. Neither model scaling nor bias-aware prompting and advanced reasoning strategies substantially mitigate these biases. These findings uncover a fundamental limitation of current multimodal architectures: deeply ingrained anatomical priors override visual evidence, posing significant risks for clinical deployment and underscoring the need for bias-aware model design and rare-case evaluation standards.

## Implications

From a clinical perspective, the observed performance gap stands as a clear warning sign: models fail to even identify easily verifiable, albeit atypical, cases. These findings suggest that VLMs should not be deployed for diagnostic tasks without explicit evaluation on atypical anatomical presentations.

From a methodological machine learning perspective, anatomical bias demonstrates a fundamental limitation in multimodal fusion architectures. Strong priors learned from internet-scale data override fine-grained visual perception, a bias mechanism consistent with findings in the general vision domain [6]. A strength of this study is its systematic evaluation of multiple mitigation strategies, including scaling model size, varying prompts, and increasing the test-time reasoning budget. Our experiments show that increasing model size does not improve performance on atypical cases, suggesting that model scale alone is insufficient to address failures on rare anatomical variants. Explicitly prompting models about the possibility of encountering rare conditions yields only modest gains on atypical cases, and no prompting strategy succeeds in closing the performance gap between typical and atypical cases. Notably, test-time reasoning provides no consistent improvements compared to the substantial gains observed on mathematical and coding tasks [13].

Two mechanisms may explain the limited effectiveness of these interventions. First, anatomical priors are deeply embedded during pretraining on billions of typical anatomy images, making them difficult to override at inference time. Second, medical images lack the step-by-step verifiability characteristic of mathematical problems; accurate diagnosis requires overriding priors at the visual perception stage, before linguistic reasoning can be applied.

## Relation to prior work

Research in the general vision domain has shown that VLMs often fail when confronted with altered depictions of familiar categories, relying on statistical priors rather than direct visual evidence [6]. To address such vulnerabilities, benchmarks such as NaturalBench have been introduced to evaluate model robustness using image-question pairs that are easy for humans but challenging for models, and to penalize responses that ignore crucial visual cues [14]. In the medical domain, the literature on visual bias in VLMs remains limited. Existing studies indicate that medical VLMs tend to exploit textual context more heavily than image content [7] and exhibit demographic biases [10, 11]. While several recent perspective papers and review articles have mentioned the potential risk of VLMs failing on rare or atypical cases [15–17], we are not aware of any study or benchmark dedicated to systematically investigating this hypothesis.

## Limitations

With the present work, we are the first to systematically investigate the performance of state-of-the-art VLMs on images of typical vs atypical anatomy.

Despite this significant progress, our benchmark only covers a fraction of atypical conditions that occur in clinical practice. Moreover, while our findings show that the models strongly rely on anatomical priors, they do not directly demonstrate that models perform worse on patients with atypical anatomy in clinically relevant tasks.

In the design of this study, we deliberately opted for basic visual perception tasks rather than questions more directly tied to medical diagnosis for two reasons. First, these tasks do not require specialized clinical expertise: any general-purpose model should be capable of determining, for example, how many fingers appear on a hand, even if it lacks advanced diagnostic capabilities. This ensures that failures cannot be attributed to missing medical knowledge but instead reflect genuine perceptual or bias-driven limitations. Second, using discrete, objectively verifiable answers allows for

robust and reproducible evaluation without the challenges associated with open-ended clinical questions. This design choice not only minimizes ambiguity in evaluation but also makes the benchmark straightforward for others to adopt, extend, and compare against.

Furthermore, to enable data sharing and ensure reproducibility, we focused exclusively on images obtained from publicly available sources. While this approach allows other researchers to replicate our findings, it introduces the possibility that some of the images in our benchmark may have been included in the training data of certain models.

An additional limitation lies in our reliance on single-image assessment, which does not capture the clinical reality of longitudinal monitoring or comparative image analysis, where radiologists often evaluate changes across multiple time points. Nevertheless, even within this simplified evaluation setting, we uncovered severe failure modes that were not solved by model scaling, prompt engineering, or increased test-time computation.

## Future Work

Several directions merit further investigation. First, *AdversarialAnatomyBench* should be expanded to encompass additional rare conditions, imaging modalities, and open-ended question formats. Complementing this expansion, future studies should examine the impact of clinical context, such as patient history and indication for imaging, on model performance, as such contextual information routinely informs clinical decision-making in practice.

From a methodological standpoint, developing effective debiasing strategies remains a critical priority. Promising approaches include architectural modifications such as visual grounding mechanisms [18] and reinforcement learning-based reasoning [19], as well as training data augmentation techniques. In particular, future research

should investigate whether augmenting training datasets with rare anatomical variants can mitigate the observed biases.

Beyond single-image evaluation, subsequent work should assess multi-image reasoning capabilities and the extent to which models can interpret temporal progression across serial imaging studies. Finally, clinical validation studies are needed to evaluate the real-world impact of these limitations in radiological workflows, including the potential benefits of radiologist-in-the-loop configurations that leverage human oversight to compensate for model shortcomings.

The broader implications of this work can be summarized as follows: Our findings underscore the need for robust rare-case evaluation as a standard requirement in medical AI deployment. For foundation model development, the results highlight that improved prompting or scaling alone is insufficient, and that architectural innovations will be required to prevent inappropriate reliance on typical-anatomy priors. From a clinical practice perspective, recognizing the limitations of VLMs when confronted with rare anatomical variants is essential to ensure safe and informed adoption. Finally, for regulatory frameworks, our findings suggest that evaluation standards should explicitly incorporate rare but clinically significant edge cases to better reflect real-world patient diversity and safeguard clinical reliability.

## Methods

### AdversarialAnatomyBench Concept

We name our medical visual question answering benchmark *AdversarialAnatomyBench*, drawing inspiration from natural adversarial examples and their emphasis on inputs that are easy for humans but challenging for models [12]. In this context, our benchmark focuses specifically on questions involving deviations from typical anatomy.

Our benchmark builds upon the following fundamental design decisions:

- **Diversity:** Images are selected to cover multiple modalities, including magnetic resonance imaging (MRI), X-ray, magnetic resonance angiography (MRA), computed tomography (CT), ultrasound, fluoroscopy, and photographs, as well as diverse regions of the body (Fig. 2).
- **Paired design:** Each atypical anatomical variant is matched with a corresponding typical reference image and evaluated using standardized perception questions, allowing direct quantification of performance gaps. Questions are formulated in a way that ensures images of atypical cases produce answers different from those observed in the majority of the population. This design choice prevents models which disregard the attached images and rely only on language priors to produce a single default answer from performing well on the benchmark [20].
- **Verifiability:** Questions are designed to allow unambiguous verification by avoiding open-ended answers in favor of categorical or numerical responses.

The benchmark uses three metrics to evaluate the models’ performance:

- **Accuracy (atypical)** measuring the accuracy on the rare anatomical variants.
- **Accuracy (typical)** measuring the accuracy on the typical cases.
- **Bias rate** [6] defined as the percentage of model answers matching the expected anatomical prior on atypical images.

Together with the metric values, we report 95% confidence intervals calculated by bootstrap stratified by question type with 1000 re-samples. Specifically, given a question set  $Q = q_1, \dots, q_{N_q}$  and a corresponding set of image sets  $X = X_{q_1}, \dots, X_{q_{N_q}}$ , for each of  $B = 1000$  bootstrap replicates, for each  $q_i$  we sample with replacement  $n_{q_i} = |X_{q_i}|$  images to form  $X_i^* = x_{i,1}^*, \dots, x_{i,n_{q_i}}^*$ . For example, for the “From the patient’s perspective, on which side of their body is the apex of their heart?” question, when computing the accuracy on atypical cases, we have 4 available images, so we sample 4 images with replacement. The full bootstrap dataset for each replicate is



obtained by concatenating across question types:  $X^* = X_1^* || \dots || X_{N_q}^*$  where  $||$  denotes concatenation. The evaluation metrics are computed on each  $X^*$ , yielding bootstrap estimates used to compute the confidence intervals.

## Data and Questions

Questions were developed collaboratively by a team of clinicians and data scientists to ensure both medical accuracy and methodological rigor. To assemble the image dataset, we systematically searched multiple online medical data repositories and publicly available datasets [21–25], and the full list of sources is provided in our repository. This process yielded 200 images spanning various regions of the body (Fig. 2) across seven imaging modalities. During curation, we manually removed any markers or annotations from images in cases where they could reveal the correct answer, such as overlays indicating the head of an embryo. All images were resized such that the longer side does not exceed 1,024 pixels while maintaining the original aspect ratio. For certain questions, such as those involving tooth counts, multiple responses could reflect anatomical bias (e.g., 28-32 teeth in the case of adult dentition); our evaluation accounts for this range when computing bias alignment.

## Models

We included 22 VLMs from the leading model families for which image understanding capabilities and model access were publicly available at the time of evaluation (see Supplementary Table 1). The selection spanned both closed-weight and open-weight systems and included general-purpose VLMs as well as a medically oriented model (MedGemma 4B). For model families offering multiple variants, we evaluated all accessible versions to enable intra-family comparison. The final set comprised models from Alibaba (Qwen3-VL series), Anthropic (Claude 4.5 series), Google (Gemini

2.5 series, Gemma 3 series, and MedGemma 4B), Meta (Llama 4 series), Mistral (Mistral 3 series), OpenAI (GPT-5 series), xAI (Grok-4), and zAI (GLM-4.5V). All models were evaluated under standardized inference parameters, with temperature set to zero where supported. Model outputs were obtained either through APIs or via locally hosted deployments, depending on availability.

## **RQ1 and RQ2 Experimental design**

The purpose of this experiment was to assess whether VLMs accurately recognize rare anatomical variants in images and whether incorrect answers align with expected anatomical biases. Each model was provided with an image accompanied by a baseline, neutral prompt: "Answer the following question based on the attached medical image: question." This prompting strategy was used consistently across all experiments unless otherwise specified. Models were instructed to output their answers in a standardized format, which was then compared against the ground truth annotations.

## **RQ3 Experimental design**

The purpose of the third experiment was to assess whether varying the models' configuration can mitigate the visual bias. To this end, we investigated three complementary strategies: Scaling, bias-aware prompting, and test-time reasoning. For all experiments, we kept the base setup from RQ1.

**Scaling experiment.** To investigate the effect of scaling model parameters on anatomical bias, we utilized the Qwen3-VL model family because it represents the current state-of-the-art among open-weight vision-language models and provides a consistent architecture across a wide range of model sizes, including the 2B, 4B, 8B, 30B, and 235B variants. The two largest variants (30B and 235B) are mixture-of-experts (MoE) architectures, and the reported parameter counts denote the total number of parameters in each model.

**Prompting experiment.** To evaluate whether alternative prompting strategies could mitigate anatomical bias, while otherwise maintaining the same experimental conditions as in RQ1, we tested two additional prompt variants:

- "Rarity-aware": "You are a medical expert. Answer the following question solely based on the attached medical image, keeping in mind that it might contain rare cases or non-standard anatomy: question."
- "Medical expert": "You are a medical expert, answer the following question solely based on the attached medical image, ignoring population biases: question."

We conducted this experiment on eight state-of-the-art VLMs spanning both closed-weight and open-weight systems: GPT-5, Gemini 2.5 Pro, Llama 4 Maverick, Grok-4, Mistral Medium 3.1, Claude 4.5 Sonnet, Qwen3-VL 235B, and GLM-4.5V.

In a separate experiment, we investigated whether allowing models to express uncertainty would reduce erroneous responses on atypical cases. To this end, we repeated the RQ1 experiment with an additional response option by appending the following suffix to the prompt: "However, if you are unsure, you may answer 'Unsure'."

**Reasoning experiment.** To investigate whether extended reasoning improves performance, we evaluated three frontier models that allowed for setting specific reasoning budgets: GPT-5, Claude Sonnet 4.5, and Gemini 2.5 Pro. Each model was tested at three levels of reasoning effort, designated as "low," "medium," and "high."

- For GPT-5, we used the model's native reasoning presets corresponding to these three levels.
- For Gemini 2.5 Pro, we configured the maximum number of reasoning tokens to 1,024, 8,192, and 24,576 for the low, medium, and high settings, respectively, following the specifications outlined in the model documentation [26].
- For Claude Sonnet 4.5, for fairness of the comparison, we matched the reasoning token counts of Gemini 2.5 Pro.

Unless otherwise specified, we report the results for the “medium” reasoning preset.

**Acknowledgements.** We thank Dr. Paul Hellerhof and Dr. Abid Irshad for allowing us to use their horseshoe kidney images and Lukas Petersson for helpful feedback. Permission was sought and obtained from Radiopaedia.org (ID:202510-0004) prior to research being undertaken. The following Radiopaedia.org images were included in our figures [27–46]. The kidney image in Fig. 1 was provided by Dr. Irshad.

P.K. discloses support for the research of this work from the Helmholtz Association under the joint research school “HIDSS4Health – Helmholtz Information and Data Science School for Health”. T. R. was supported by a scholarship from the Hanns Seidel Foundation with funds from the Federal Ministry of Education and Research Germany (BMBF). F.R.K. receives support from the German Cancer Research Center (CoBot 2.0), the Joachim Herz Foundation (Add-On Fellowship for Interdisciplinary Life Science), the Central Indiana Corporate Partnership AnalytiXIN Initiative, the Evan and Sue Ann Werling Pancreatic Cancer Research Fund, and the Indiana Clinical and Translational Sciences Institute (EPAR4157) funded, in part, by Grant Number UM1TR004402 from the National Institutes of Health, National Center for Advancing Translational Sciences, Clinical and Translational Sciences Award. The content is solely the responsibility of the authors and does not necessarily represent the official views of the National Institutes of Health. A.R. discloses support for the research of this work from the Helmholtz Association of German Research Centers in the scope of the Helmholtz Imaging Incubator (HI).

## Competing interests

F.R.K. declares advisory roles for Radical Healthcare, USA; and the Surgical Data Science Collective, USA.

## References

- [1] Bubshait, D. K. A review of polydactyly and its inheritance: Connecting the dots. *Medicine* **101**, e32060 (2022).
- [2] Taghavi, K., Kirkpatrick, J. & Mirjalili, S. The horseshoe kidney: surgical anatomy and embryology. *Journal of pediatric urology* **12**, 275–280 (2016).
- [3] Eitler, K., Bibok, A. & Telkes, G. Situs inversus totalis: a clinical review. *International journal of general medicine* 2437–2449 (2022).
- [4] Royer, C., Menze, B. & Sekuboyina, A. Multimedeval: A benchmark and a toolkit for evaluating medical vision-language models. *arXiv preprint arXiv:2402.09262* (2024).
- [5] Zhou, T. *et al.* Drvd-bench: Do vision-language models reason like human doctors in medical image diagnosis? *arXiv preprint arXiv:2505.24173* (2025).
- [6] Vo, A. *et al.* Vision language models are biased. *arXiv preprint arXiv:2505.23941* (2025).
- [7] Buckley, T., Diao, J. A., Rajpurkar, P., Rodman, A. & Manrai, A. K. Multimodal foundation models exploit text to make medical image predictions. *arXiv e-prints arXiv-2311* (2023).
- [8] Gu, Y. *et al.* The illusion of readiness: Stress testing large frontier models on multimodal medical benchmarks. *arXiv preprint arXiv:2509.18234* (2025).
- [9] Sadanandan, B. & Behzadan, V. Vsf-med: A vulnerability scoring framework for medical vision-language models. *arXiv preprint arXiv:2507.00052* (2025).

- [10] Yang, Y. *et al.* Demographic bias of expert-level vision-language foundation models in medical imaging. *Science Advances* **11**, eadq0305 (2025).
- [11] Xu, S., Janizek, J. D., Jiang, Y. & Daneshjou, R. *Biasicl: In-context learning and demographic biases of vision language models*, 88–97 (Springer, 2025).
- [12] Hendrycks, D., Zhao, K., Basart, S., Steinhardt, J. & Song, D. *Natural adversarial examples*, 15262–15271 (2021).
- [13] Guo, D. *et al.* Deepseek-r1: Incentivizing reasoning capability in llms via reinforcement learning. *arXiv preprint arXiv:2501.12948* (2025).
- [14] Li, B. *et al.* Naturalbench: Evaluating vision-language models on natural adversarial samples. *Advances in Neural Information Processing Systems* **37**, 17044–17068 (2024).
- [15] Shrestha, P., Amgain, S., Khanal, B., Linte, C. A. & Bhattarai, B. Medical vision language pretraining: A survey. *arXiv preprint arXiv:2312.06224* (2023).
- [16] Lin, H., Xu, C. & Qin, J. Taming vision-language models for medical image analysis: A comprehensive review. *arXiv preprint arXiv:2506.18378* (2025).
- [17] Handler, R., Sharma, S. & Hernandez-Boussard, T. The fragile intelligence of gpt-5 in medicine. *Nature Medicine* 1–3 (2025).
- [18] Chen, K. *et al.* Think twice to see more: Iterative visual reasoning in medical vlms. *arXiv preprint arXiv:2510.10052* (2025).
- [19] Pan, J. *et al.* *Medvlm-r1: Incentivizing medical reasoning capability of vision-language models (vlms) via reinforcement learning*, 337–347 (Springer, 2025).

- [20] Goyal, Y., Khot, T., Summers-Stay, D., Batra, D. & Parikh, D. *Making the v in vqa matter: Elevating the role of image understanding in visual question answering*, 6904–6913 (2017).
- [21] <https://radiopaedia.org/>. [Accessed 27-11-2025].
- [22] Irvin, J. *et al.* *Cheexpert: A large chest radiograph dataset with uncertainty labels and expert comparison*, Vol. 33, 590–597 (2019).
- [23] Rajpurkar, P. *et al.* Mura: Large dataset for abnormality detection in musculoskeletal radiographs. *arXiv preprint arXiv:1712.06957* (2017).
- [24] Brahmi, W. & Jdey, I. Automatic tooth instance segmentation and identification from panoramic x-ray images using deep cnn. *Multimedia Tools and Applications* **83**, 55565–55585 (2024).
- [25] Brahmi, W., Jdey, I. & Drira, F. Exploring the role of convolutional neural networks (cnn) in dental radiography segmentation: A comprehensive systematic literature review. *Engineering Applications of Artificial Intelligence* **133**, 108510 (2024).
- [26] Gemini API documentation. <https://ai.google.dev/gemini-api/docs/openai>. Accessed: 2025-11-02.
- [27] Jones, J. Accessory premolar teeth. *Case study, Radiopaedia.org* (2013). URL <http://doi.org/10.53347/rID-22225>.
- [28] Uribe, S. Normal orthopantomography (opg). *Case study, Radiopaedia.org* (2016). URL <http://doi.org/10.53347/rID-46431>.
- [29] Singh, G. Situs inversus with pneumothorax. *Case study, Radiopaedia.org* (2010). URL <http://doi.org/10.53347/rID-8495>.

- [30] Bickle, I. Normal chest radiograph - female. *Case study, Radiopaedia.org* (2015). URL <http://doi.org/10.53347/rID-33225>.
- [31] Schubert, R. Aberrant right subclavian artery - mr angiography. *Case study, Radiopaedia.org* (2011). URL <http://doi.org/10.53347/rID-13708>.
- [32] Gaillard, F. Normal mra of the aortic arch. *Case study, Radiopaedia.org* (2015). URL <http://doi.org/10.53347/rID-35881>.
- [33] Hacking, C. Beaver tail liver (2015). URL <http://doi.org/10.53347/rID-39317>.
- [34] Di Muzio, B. Amiodarone hepatotoxicity. *Case study, Radiopaedia.org* (2012). URL <http://doi.org/10.53347/rID-19223>.
- [35] Santizo Castillo, J. C. Supernumerary kidney. *Case study, Radiopaedia.org* (2022). URL <http://doi.org/10.53347/rID-97733>.
- [36] Dixon, A. Normal ct abdomen (2015). URL <http://doi.org/10.53347/rID-36677>.
- [37] Qureshi, P. A. A. A. Macrodystrophia lipomatosa. *Case study, Radiopaedia.org* (2018). URL <http://doi.org/10.53347/rID-60654>.
- [38] Al Salam, H. Macrodystrophia lipomatosa (2009). URL <http://doi.org/10.53347/rID-7609>.
- [39] Pai, V. Incomplete double ureter. *Case study, Radiopaedia.org* (2014). URL <http://doi.org/10.53347/rID-26900>.
- [40] Niknejad, M. T. Normal intravenous urography. *Case study, Radiopaedia.org* (2020). URL <http://doi.org/10.53347/rID-85286>.
- [41] Knipe, H. Dichorionic tri-amniotic (dcta) triplets. *Case study, Radiopaedia.org* (2015). URL <http://doi.org/10.53347/rID-36543>.



- [42] Lukies, M. Normal first trimester pregnancy (2023). URL <http://doi.org/10.53347/rID-76936>.
- [43] Khurfan, B. Tibial hemimelia. *Case study, Radiopaedia.org* (2021). URL <http://doi.org/10.53347/rID-86822>.
- [44] Liew, G. Normal tibia fibula x-rays - 10-year-old. *Case study, Radiopaedia.org* (2023). URL <http://doi.org/10.53347/rID-163734>.
- [45] Elthokapy, M. M. Accessory navicular bones bilaterally. *Case study, Radiopaedia.org* (2021). URL <https://doi.org/10.53347/rID-93839>.
- [46] Ranchod, A. I. Splay feet. *Case study, Radiopaedia.org* (2023). URL <https://doi.org/10.53347/rID-170048>.

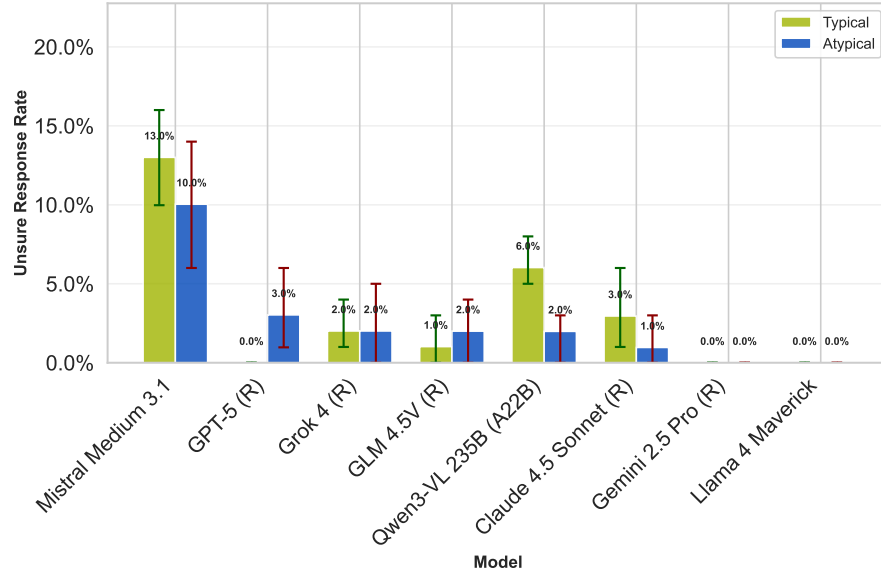
## Supplementary material

Organization	Name	Medical	Access	Model Size
Alibaba	Qwen3-VL 235B	No	Open	235B (A22B)
	Qwen3-VL 30B	No	Open	30B (A3B)
	Qwen3-VL 8B	No	Open	8B
	Qwen3-VL 4B	No	Open	4B
	Qwen3-VL 2B	No	Open	2B
Anthropic	Claude 4.5 Sonnet (R)	No	Closed	-
	Claude 4.5 Haiku (R)	No	Closed	-
Google	Gemini 2.5 Pro (R)	No	Closed	-
	Gemini 2.5 Flash (R)	No	Closed	-
	Gemini 2.5 Flash Lite (R)	No	Closed	-
	Gemma 3 27B	No	Open	27B
	Gemma 3 4B	No	Open	4B
	MedGemma 4B	Yes	Open	4B
Meta	LLama 4 Maverick	No	Open	400B (A17B)
	LLama 4 Scout	No	Open	109B (A17B)
Mistral	Mistral Medium 3.1	No	Closed	-
	Mistral Small 3.2 24B	No	Open	24B
OpenAI	GPT-5 (R)	No	Closed	-
	GPT-5 mini (R)	No	Closed	-
	GPT-5 nano (R)	No	Closed	-
xAI	Grok 4 (R)	No	Closed	-
zAI	GLM 4.5V (R)	No	Open	106B (A12B)

**Table 1 Model Overview.** Our evaluation included 22 models from leading model families and included both open and closed-weight models of varying sizes. Reasoning models are denoted with (R) and the numbers in parentheses in the “Model Size” column provide the active parameter count for case of mixture-of-experts (MoE) models.

Model	↑ Accuracy (atypical)	↑ Accuracy (typical)	↓ Bias rate
GPT-5 (high) (R)	42.0% (37.0%, 48.0%)	84.9% (79.0%, 90.0%)	45.0% (38.0%, 51.0%)
GPT-5 (medium) (R)	43.0% (37.0%, 49.0%)	79.9% (74.0%, 86.0%)	49.1% (42.0%, 55.0%)
GPT-5 (low) (R)	42.0% (36.0%, 48.0%)	78.9% (73.0%, 85.0%)	48.0% (41.0%, 54.0%)
Gemini 2.5 Pro (high) (R)	44.0% (37.0%, 50.0%)	83.0% (77.0%, 89.0%)	51.0% (44.0%, 58.0%)
Gemini 2.5 Pro (medium) (R)	40.0% (34.0%, 46.0%)	81.0% (76.0%, 86.0%)	50.0% (43.0%, 57.0%)
Gemini 2.5 Pro (low) (R)	42.0% (37.0%, 48.0%)	82.9% (78.0%, 88.0%)	52.1% (45.0%, 58.0%)
Claude 4.5 Sonnet (high) (R)	27.0% (23.0%, 31.0%)	78.9% (73.0%, 84.0%)	69.1% (64.0%, 74.0%)
Claude 4.5 Sonnet (medium) (R)	26.0% (21.0%, 31.0%)	81.1% (75.0%, 86.0%)	69.0% (64.0%, 75.0%)
Claude 4.5 Sonnet (low) (R)	28.9% (25.0%, 32.0%)	76.1% (70.0%, 82.0%)	66.1% (62.0%, 70.0%)

**Table 2 Reasoning experiment results.** Increased amount of reasoning does not result in improved performance on atypical cases. Reasoning models are denoted with (R).



**Fig. 1 Models rarely choose to answer with “Unsure” when provided with a possibility to do so.** The unsure answer is chosen only in up to 13% of typical (green) and 10% atypical (blue) cases, with some models, including Gemini 2.5 Pro and Llama 4 Maverick never providing unsure responses. Reasoning models are marked with (R).